MULTISCALE ANALYSIS OF SAR FROM THE EARTH SURFACE.

J.M. Redondo(1) A. Tarquis(2), A. Matulka(1) and A. Platonov(1)

1-Departament de Fisica Aplicada, B5 Campus Nord
Univ. Politecnica de Catalunya, 08034, Barcelona, Spain., redondo@fa.upc.edu.
2- Departament de Matematica Aplicada. E.T.S.Ing. Agronomos, UPM, Madrid. Spain.

ABSTRACT

The use of Synthetic Aperture Radar (SAR) to investigate the earth's surface provides a wealth of useful information. Here we will discuss some recent fractal and multi-fractal techniques used to identify oil spills and the dynamic state of the Ocean as well as the mountain structures in the solid earth. It is important both in the Ocean and in the Atmosphere to be able to parametrize mixing at the Rossby Deformation Radius scale (*i.e.* most energetic eddy scale) to aid in the prediction of pollutant dispersion. Results presented here aim to identify different SAR signatures and at the same time provide calibrations for the different local configurations that allow to predict the behaviour of different tracers in the sea surface, in the atmosphere or in the earth. We also compare different SAR images of the Eastern Pyrenees, evaluating the changes in structure as a function of average height. The multiple correlations between HH HV VV polarizations and the images are used to calculate the fractal dimension with the Box-Counting method. The distribution of the boxes is accomplished systematically for each SAR intensity level, ρ the intersection of these boxes with the images gives $N(\rho)$ boxes with a non void intersection, which may be compared with the standard multifractal formalism.

1. INTRODUCTION

The diffusion of oil spills and slicks in the ocean (Figure 1) have been investigated using several multi-fractal and geometrical techniques developed by the authors [1-5]. Different cases are studied analyzing mixedness, diffusivity and multifractality [2]. It has to be taken into account, nevertheless that the SAR and ASAR sensors have certain limitations depending on the range of local winds over the ocean surface, either with very small winds of less than about (2 m/s) or with very high wind speed (above approx. 12 m/s) oceanic surface films cannot, or may only barely, be identified [6-8], this prevents routine observations in regions of high winds as the north Atlantic, but for the Mediterranean Sea, or other European coastal waters, the conditions are good most of the times [6,7]. On other hand, the sunshine illumination conditions are not a limiting factor for the acquisition of SAR images as the cloud cover is transparent for SAR sensors. The nocturnal conditions are not limiting either because SAR is an active sensor that radiates its own energy. These effects allow us to use remote sensing of the ocean surface and even to monitor and police pollution from space. Here we will discuss several techniques that are able to extract geometrical information from the ocean surface (Figures 1 and 2) linked in several ways to the dynamics of a certain area. Here we will describe the formal relationships between the multi-fractal parameters applying them to SAR images of the ocean and the earth surface, in sections 2 and 3

2. TOPOLOGICAL FRACTAL MEASURES

Fractals are geometric entities that present self-similarity and they are often the result of iterative processes such as turbulence. The self-similarity implies that if we have observations from different scales the results are similar, although in natural systems it is enough to have only a certain statistical similarity [3]. These natural entities have usually anisotropic nature and then there may be different scaling laws for the different directions. Examples of these are the surface topography and the clouds, where the vertical coordinate has a smaller magnitude that horizontal coordinates due to stratification [9-10]. Fractal analysis is a very useful geometrical tool to characterize these objects in which an additional possibility is the calculation of the corresponding fractal dimension along the different coordinates so it may also reflect the anisotropic scaling. The eddies can also be detected from SAR (Figures 3 and 4) as well as the local self-similarity [11-14].

Usually, the detected oil spills by SAR have an elongated structure as these are shed from the ships in motion as they clean their ballast tanks. As turbulent diffusion acts on the plume formed by pollutants, these mix and therefore entrain seawater, so there is a measurable widening of the width of the spill. The natural oil slicks do not have these Euclidean, linear characteristics; the natural organic matter sources are not point sources and they have a diffuse initial character related to both the local currents, turbulence and the zoo and phytoplankton fields, fishery flocks, suspended or floating debry, etc[11,12]. Man-made recent oil spills and other tensioactive products detected in the sea surface by SAR images, have two general peculiarities that seem universal. A well defined axis indicating the advected continuous spill, with a tendency along the spill to increase its thickness. Due to mass conservation and the application of the diffusion process (Fick's Law). At the same time, there is a significant decrease of the concentration (intensity of the grey tones) along its length due to the turbulent diffusion and other non-lineal processes.

The analysis made with DigImage and Imacal [11,3]software on the intensity of the grey tones of the selected areas that exhibit the typical spiral features of the natural oil slicks shows the self-similarity character of their mesoscale spatial distribution (Figure 4) and also their fractional dimension character, which may be defined either for each intensity value
or for the contours separating two neighbour intensity values. This constitutes an array of superposed set of fractal objects which we may analyze in a variety of ways. It has to be noted, though, that it is not possible in all cases to deduce the dynamics that lead to the observations. Nevertheless we may assert certain predictive conclusions comparing different surface features with multi-fractal analysis and here we will just comment a few examples, The basis theoretical justification [3-7] consists in relating the scalar equivalent to the turbulence energy spectrum as a Fourier transform of the correlation, also directly related to the second order structure function. We suppose that the surface flow will advect the surface structures.
The box-counting algorithm divides the embedding Euclidean plane in smaller and smaller boxes (e.g., by dividing the initial length l_0 by n, which is the recurrence level of the iteration). For each box of size l_0/n it is then decided if the convoluted line, which is analyzed, is intersecting that box. Finally, is plotted N versus the size of the box e in a log-log plot, and the slope of that curve, within reasonable experimental limits, gives the fractal dimension for a single intensity or for a group of similar SAR backscatter intensities. This method of box-counting is used in ImaCalc software [3,11] used to detect the self-similar characteristics for different SAR image grey intensity levels and to identify different sea surface dynamic processes. Each of the intensity values may reflect different physical processes and lead to a different value of its fractal dimension. This entity will exhibit a range of values of $D(\rho)$ 0-2 for each SAR intensity.

Figure 1. Example of an oil spill.

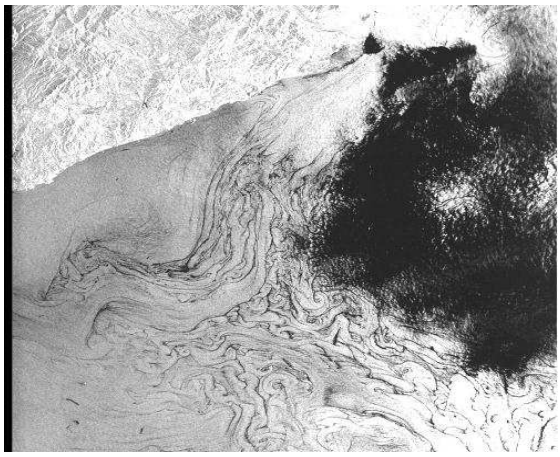

Figure 2. Complex eddy patterns detected by SAR in the NW Mediterranean sea.

Fractals are geometric entities that present self-similarity and they are often the result of iterative processes such as turbulence. The self-similarity implies that if we accomplish observations from different scales the results are similar, although in natural systems it is enough to have only a certain statistical similarity. These entities have usually anisotropic nature and then there may be different scaling laws for the different directions. Examples of these are the surface topography and the clouds, where the vertical coordinate has a smaller magnitude that horizontal coordinates due to stratification. Fractal analysis is a very useful tool to characterize these objects in which an additional possibility is the calculation of the corresponding fractal dimension along the different coordinates so it may also reflect the anisotropic scaling.

The theory applied here links fractal analysis to the turbulence self-similarity [11-13]. Turbulent diffusivities and Richardson's Law applied to the ocean surface. If V is a variance at scale δ

$$V(\delta) = V(0) - \frac{S^2(\delta)}{2} = < (\rho(x+\delta)\rho(x))^2 > \quad (1)$$

The self similar character of the signal, that for velocity differences was popularized in [Kolmogorov, 1941] through the use of structure functions may scale through the Hausdorff dimension H when the limit

$$Lim_{\delta \to 0} \quad \frac{< (\rho(x+\delta) - \rho(x)) >}{\delta^H} \qquad (2)$$

Converges, showing the scaling dependence for a fractal set, either in space or in the form of a time series (when the coordinate is time and instead of a wave-number we have a period).

With the stated conditions, the variance of the signal under study will show a scale dependency such than $V(\delta) \approx \delta\, 2H$ [,].

Using $\delta = 2\pi/k$ and the description of the spatial spectral density function, *E(k),* we have equivalently spectral information.

$$E(\delta) \approx \delta^{\beta} \qquad (3)$$

and relating the scalar equivalent to the turbulence energy spectrum as a Fourier transform of the correlation, also directly related to the second order structure function as

$$S^2(x,\delta) = <\rho^2(x,\delta)> = V - \tfrac{1}{2} <(\rho(x+\delta) - \rho(x))^2> \quad (4)$$

We may write in terms of the spatial equivalent to the turbulent energy density

$$E(k)\, \alpha\, \delta \int_0^{\delta} \rho^{\,2}(x)\, e^{ikx}\, dx \approx \delta V \qquad (5)$$

so relating the Euclidean, Fractal and Hausdorff dimensions, using that *(H = E – D)*

$$E(k) \approx \delta V \approx \delta^{2H+1} \approx \delta^{2E+1-2D} \qquad (6)$$

Thus the relationship between the exponent of the spectral density function and the fractal dimension may be written as:

$$\beta = 2E + 1 - 2D \qquad (7)$$

3. THEORY OF MULTI-FRACTALS

The measurement of multifractals is mainly the measurement of a statistic distribution which is why the results yield useful information even if the underlying structure does not show a self similar or self affine behavior.

For a monofractal object, the number n of features of a certain size δ varies as

$$n(\delta) \propto \delta^{-D_0} \quad , \qquad (8)$$

where the fractal dimension D_0

$$D_0 = \lim_{\delta \to 0} \frac{\log n(\delta)}{\log \frac{1}{\delta}} \qquad (9)$$

can be measured by counting the number n of boxes needed to cover the object under investigation for increasing box sizes δ and estimating the slope of a log-log plot.

There are several methods for implementing multifractal analysis; here the moment method is explained. This method use mainly three functions: $\tau(q)$, the mass exponent function, α, the coarse Hölder exponent, and *f(α)*, the multifractal spectrum. For a measure (or field) defined in a two-dimensional support of the $L \times L$ pixels image, μ (grey tone from 0 to 255), it could be spatially decomposed in terms of infinitely many intertwined sets of fractal dimensions. If that is the case, one fractal dimension cannot characterize all the complexity and several fractal dimensions will be estimated depending on the position.

Applying box counting "up-scaling" partitioning process we can get the partition function $\chi(q,\delta)$ defined as:

$$\chi(q,\delta) = \sum_{i=1}^{n(\delta)} \mu_i^q(\delta) = \sum_{i=1}^{n(\delta)} m_i^q \qquad (10)$$

Where m is the mass of the measure, q is the mass exponent, δ is the length size of the box and $n(\delta)$ is the number of boxes in

which $m_i > 0$. Based on this, the mass exponent function ($\tau(q)$) shows how the moments of the measure scales with the box size:

$$<\tau(q)>=\lim_{\delta\to 0}\frac{\log<\chi(q,\delta)>}{\log(\delta)}=\lim_{\delta\to 0}\frac{\log<\sum_{i=1}^{n(\delta)}m_i^q>}{\log(\delta)} \quad (11)$$

where <> represents statistical moment of the measure defined on a group of non overlapping boxes of the same size partitioning the area studied. D_q are related as:

$$\tau(q)=(1-q)D_q \quad (12)$$

This characterization of multifractal measures is the concept of generalized dimensions Dq, which corresponds to the scaling exponents for the qth moment of the measure. Based on the work of Rényi; are defined as:

$$D_q=\lim_{\delta\to 0}\frac{1}{1-q}\frac{\log\sum_{i=1}^{n(\delta)}m_i^{\,q}}{\log\delta} \quad (13)$$

The sum in the numerator of Equation 13 is dominated by the highest values of pi for q > 0, and by the lowest values of pi for q < 0.

The singularity index (α) can be determined by Legendre transformation of the $\tau(q)$ curve [as:

$$<\alpha(q)>=\frac{d<\tau(q)>}{dq} \quad (16)$$

The number of cells of size δ with the same α, $n_\alpha(\delta)$, is related to the cell size as $n_\alpha(\delta) \propto \delta^{-f(\alpha)}$, where $f(\alpha)$ is a scaling exponent of the cells with common α. Parameter $f(\alpha)$ can be calculated as:

$$<f(\alpha)>=q<\alpha(q)>-<\tau(q)> \quad (17)$$

Multifractal spectrum (MFS), a graph of α vs. $f(\alpha)$, quantitatively characterizes variability of the measure studied with asymmetry to the right and left indicating domination of small and large values respectively. The width of the MF spectrum indicates overall variability.

MFA in 2-D images involves partitioning the plane into boxes to construct samples with multiple scales. The box-counting method combines pixels to form larger mutually exclusive boxes each containing different set of pixels. If we have an image of $L\times L$ pixels and a partitioned process is applied with a box size $\delta\times\delta$ then the number of boxes with linear size δ ($n(\delta)$) will follow the proportion:

$$n(\delta)\propto\left(\frac{L}{\delta}\right)^2 \quad (18)$$

The bigger δ is, the smaller the number of samples, so the statistical analysis might not be accurate enough.

To calculate the fractal dimension, the Box-Counting method used produces a coverage of the object and the simplest method is to characterize it with boxes of side e. For the plane these boxes will be square and for an object in space they will be cubes. The distribution of the boxes is accomplished systematically, the intersection of these with the object carries the fact that we have *N* boxes with a non void intersection Already we have some values of *N* and , but as they are not exactly the result of the better coverage possible it may be applied the concept of self-similarity and thus the basic covering is accomplished repeating the process for many different possible diminishing observation scales.

When we work with real images they do not have generally some perfectly defined contours, but we have some wide quite ranges of scalar intensity values to process. If we group the available data and describe them by a single large set and calculate the fractal dimension we then lose the corresponding information due to the intensity variation.

It is also possible to accomplish a segmentation in many intervals that contains each one a very well defined intensity range. For each one of these ranges it will be applied the usual fractal dimension calculation with the box-counting method and we will obtain the corresponding fractal dimension for each intensity level. The result of the process will be a set of dimension values, function of the intensity.

The fractal dimension *D(ρ)* is a function of intensity and may be calculated using

$$D(\rho)=-\frac{\log N(\rho)}{\log\lambda} \quad (19)$$

where *N(ρ) i*s the number of boxes of size λ needed to cover the SAR contour of intensity *ρ*.

The box-counting algorithm divides the embedding Euclidean plane in smaller and smaller boxes (e.g., by dividing the initial length λ_0 by n, which is the recurrence level of the iteration). For each box of size λ_0/n it is then decided if the convoluted line, which is analyzed, is intersecting that box. Finally, is plotted N versus λ_0/n (i.e., the size of the box e) in a log-log plot, and the slope of that curve, within reasonable experimental limits, gives the fractal dimension. This method of box-counting is used in [3] to detect the self-similar characteristics for different SAR image grey intensity levels ρ . Each of the intensity values may reflect different physical processes and lead to a different value of its fractal dimension, this entity can be either fractal or not, but exhibits a range of values 0-2 for each intensity.

With this application we can define the image region of interest, select an intensity range to analyze and execute the multi-fractal characterization process in a simple iterative way. In the right side of figure 3, other smaller graphs show the observed dimension values as a grey-level function of the characterized intervals.

In addition to the direct visualization of the data, the results are also are kept in a file in order to be analyzed independently with external tools, The formats of the images and other import-export abilities of the program ImaCalc are very wide and it may be run under Windows or Unix environments.

Using the traditional energy spectra used in turbulence studies characterized by a single power law within the inertial sub-range (defined as the range of scales where production and dissipation of energy, ε are in local balance) we may use a theoretical relationship between the turbulence spectral slope and the fractal dimension, we are now able to apply it to a spatial spectrum as described above, and define a global fractal dimension using directly the spectral analysis on the radial distribution of intensity values of a SAR image

With this methodology a unique value is obtained that characterizes the overall spatial fractal dimension of the system. The steps are described as follows: make an image segmentation to obtain the interest region.(ρ_{mn} , m and n are the x-y discrete coordinates). Compute the FT (Fourier Transform) to obtain the frequency spectrum representation. (I_{uv} , u and v are the frequency discrete coordinates). Compute the square of the signal intensity or energy S_v with: $S_v=|\rho_{uv}|^2$. Obtain the *radia spectral* representation, as the radial distribution of S_{uv} and finally find the exponent β from $S_r = r^{-\beta}$. Using the radius as an isotropic lengthscale. With a linear fit from a log-log representation, we may obtain the spatial spectral value of the set of all SAR image intensities, which we assume is also β and using as the Euclidean dimension E = 3 and the fractal dimension relationship we have:

$$D = \frac{7-\beta}{2} \qquad (20)$$

The program ImaCalc performs interactively most of the multi-fractal box counting methods as well as the spectral ones. Different regions may be equalized depending on their intensity histogram distribution. Figure 3 shows the dialog box with the zoom, histogram and a fractal fit.

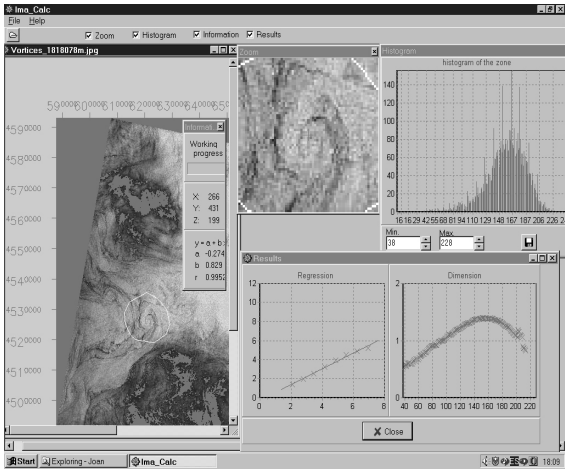

Figure 3. Multifractal $D(\rho)$ curves, Histogram, zoom, Pdf for different features in SAR images of a vortex.

Experimental observations of SAR features are investigated with multi-scale fractal techniques in order to extract relevant information on the spectral characteristics of mixing and diffusive events. Both density and tracer marked oil spills and slicks are investigated in detail using third order structure function analysis that indicates strong inverse cascades towards the large scales producing spectral variations [4]. The different local mixing processes are compared by mapping their different multifractal scaling. Other multifractal measurements can also be related to physical mechanisms that affect in a different fashion the different scalar intensities used to identify the flows, as in [ ] where

stratification is shown to affect clearly the maximum fractal dimension.

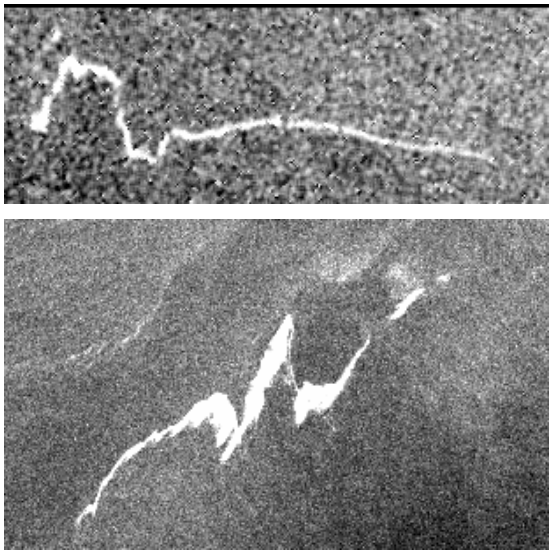

Figure 4. Example of inverted ERS-1 SAR image with surface features in the Northwest Mediterranean

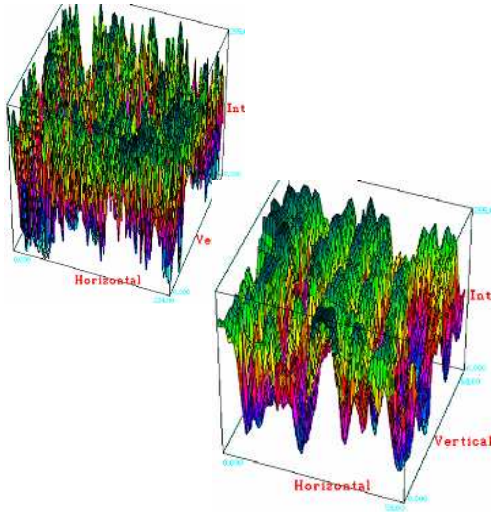

Figure5. Comparison of the structure in 3D False colour of antropogenic oil spills and natural slicks detected by SAR in the NW Mediterranean sea.

4. RESULTS

Examples of the image enhancement and of the techniques used to reveal the structure of the oil slicks and spills detected by the reduction in surface roughness of the ocean are presented. Figure 4 shows an enhanced SAR image with two typical examples where a combination of oil spills and natural slicks are present, In figure 5, the spatial distribution of SAR intensity pixels (about 4 x 10^4 m^2 per pixel) in a 3D representation, with the third coordinate indicating the actual local value of the SAR intensity may be used to distinguish the type of structure. For multifractal measurements, a probability distribution is measured. In practice, using the box counting method, for every box the probability of "containing the object", or in this application, the values of a certain SAR reflectivity, is also called the partition function, which may be obtained for different moments q which can vary from -8 to +8 .

The well known multifractal function *f(a)* [2] may be seen as the fractal dimension of the set of intervals that corresponds to a singularity a, and a graph of *a* vs. *f(a)* is called the multifractal spectrum of the measure. A measure is multifractal when its multifractal spectrum exists and has the shape of an inverted parabola. A generally equivalent way to describe a multifractal scaling is by considering the scaling laws of the moments of the measure.

In practice, the object density is taken to the respective power of *q*, summed for all *i,* and plotted versus the box size in a log–log coordinate system. From the slope, which is also called the mass exponent t, the generalized dimensions are estimated as $D(q)=t(q) / (1- q)$.

With SAR images from the ocean surface we cannot rely strictly on theoretically limit for the calculation of the fractal, non- fractal or multifractal behaviour, because they have a finite size, and we have assigned a fixed range of values to the different SAR reflectivity intensity. The range of scale boundaries are defined by the image resolution, and we use numerical log/log fits (which tend to straighten any curve) to obtain the Rényi dimensions.

In order to compare the two multifractal analysis procedures involving either a single fractal measure for each of the intensity levels (or grouped in sets) with the moment calculation for the generalized dimensions, we checked the numerical values at each algorithm step. Outside of this scale range, the theoretical values of *D(q)* (calculated as the limit when the scale approaches zero) and the numerical values of *D(q)* (calculated from the regression fits). They are still very close if we select the range of scale and a grid matching the theoretical generation pattern. We applied this for a range of oil spill images as well as for different terrain types.

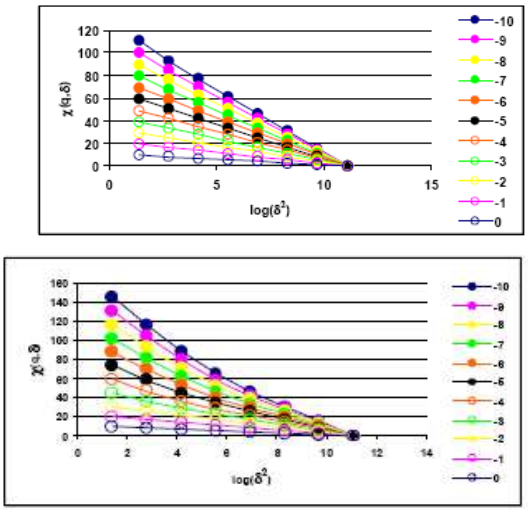

Figure 6. Range of functions $\chi(q,\delta)$ for a recent, (above) oil spill and for a weathered one (below).

A modified partition function of all images for 0=q=10 over box sizes e ranging from 1 to 512 pixels based on the square of the grey levels has been used. The mass exponent t is estimated as the slope of the log/log data for the SAR image showing the optimized box size range.

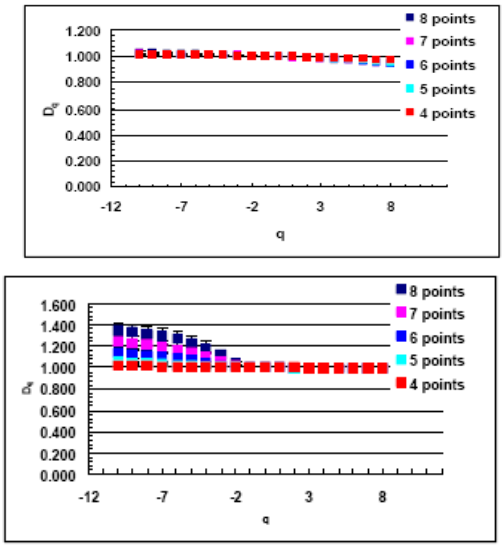

Figure 7. Generalized dimensions *(Dq)* obtained for a recent and a weathered oil spill, showing the low values of the fractal dimension

Figure 6 shows the procedure described in section 3 for a recent and a weathered oil spill. In ofder to enhance the range of scales, $\chi(q,\delta)$ are shown against the square of the intensity value, and in figure 7 the values of the generalised dimensions *Dq,* this may be compared with results of [12-14] where similar features are compared.

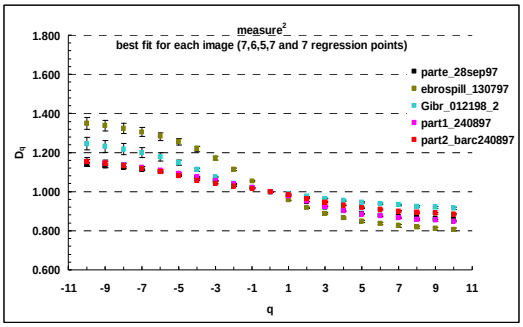

Figure 8. Normalized multifractal patterns exhibited by natural slicks and oil spills.

The correlations of intensity values and the radial integral of these, indicates the spatial scale *l* where the SAR intensities are well correlated. If we suppose that the surface currents are responsible (at least partly) for the spatial distribution of the ocean roughness for two main reasons, first the slope at both sides of an eddy is very different at producing radar backscatter from a side (as happens with ERS-1/2 and also ENVISAT and RADARSAT)

For example, the oil spill shown in figure 1, at a higher resolution using ASAR would correspond to a range of non- dimensional times T_{oil} between 0.7 and 0.8 matching the fractal dimension of 1.3-1.4. There are other indications that may be useful from the SAR observations, such as the low local wind at the time the image was taken. There is a consistent pattern that distinguishes the recent oil spills and the natural slicks that have adapted to the multi-scale turbulent flow of the ocean surface. Figure 8 show some of the differences between recent, characterized by the low fractal dimension of low SAR reflectivity values, and weathered oil spills or slicks. .As an example from [6]. Local average diffusivities derived from SAR observations are also possible using Richardson's law to different sizes of spills, which will comply with the 4/3 law. Both numerical simulations [4, 5] and laboratory experiments confirm the conditions for diffusion under the Weillburn distribution of prevailing winds.

5 CONCLUSIONS

There is a need to calibrate the different regions determining the distribution of meso-scale vortices of size the Rossby deformation scale and other dominant features. Multi-fractal analysis can be used to distinguish fresh oil spills and natural slicks in the ocean surface. The SAR images exhibited a large variation of natural features produced by winds, internal waves, the bathymetric distribution, by convection, rain, etc as all of these produce variations in the sea surface roughness so that the topological changes may be studied and classified [10-13]. In a similar way topography may be studied with the methodology described in section 3. An additional unique value is obtained that characterizes the overall spatial fractal dimension of the system integrating the multifractal functions. Several polarizations of the SAR have b compared exhibiting their different structure functions [14-17] up to 6th order. The flatness or Kurthosis is a statistic parameter which indicates the shape of the pdfs of the SAR intensity, and seems to be a very good indicator of the degree of existing structure; when flatness changes with scale following a potencial law, intermittency is present. Both the multifractal spectra and the distribution of the Flatness function F are found to be useful to measure intermittency, when it is applied to the correlations between the different SAR polarizations. Comparisons with the standard multifractal formalism [2, 15] also may reveal the importance of anisotopy.

The authors thank the ENV4-CT96-0334 European Union Project, INTAS, ISTC1481, and ESA-IP2240 as well as MEC projects SB2000-0076 and ESP2005-07551.

7. REFERENCES

1. Redondo J.M. and Garzon G(2004).Multifractal structure and intermittency in Rayleigh-Taylor Driven Fronts". Ed. S. Dalzielwww.damtp.cam.ac.uk/iwpctm9/proceedings/IWPCTM9/Papers/Programme.htm.

2. Dathe, A., Perrier, E., Tarquis, A., (2006). Multifractal análisis of two-dimensional soil porous structure on natural images. Geoderma 134, 318–326.

3. Grau J. (2004) PhD Thesis. Univ. Politecnica de Catalunya, UPC, Teseo, Barcelona.

4. Castilla R, Redondo J.M., Gamez P.J., Babiano A. (2007) Coherent vortices and Lagrangian Dynamics in 2D Turbulence. *Non-Linear Processes in Geophysics* 14. 139-151.

5. Redondo J.M. (2002). Mixing efficiencies of different kinds of turbulent processes and instabilities, Applications to the environment. in *Turbulent mixing in geophysical flows.* Eds. Linden P.F. and Redondo J.M. 131-157.

6. G.W. Jolly, A. Mangin, F. Cauneau, M. Calatuyud, V. Barale, H. M. Snaith, O.Rud, M. Ishii, M. Gade, J. M. Redondo and A. Platonov (2000) Clean Seas Project. *Final Report* ENV4-CT96-0334. Brusels..

7. M.O. Bezerra, M. Diez, C. Medeiros, A. Rodriguez, E. Bahia., A. Sanchez-Arcilla and J.M. Redondo (1998). Study on the influence of waves on coastal diffusion using image analysis. *Journal Flow, Turbulence and Combustion*. 59,.191-204.

8. J.M. Redondo (1994). Turbulent mixing in the Atmosphere and Ocean. Fluid Physics. 584-597. World Scientific. New York.

9. J.M. Redondo and Linden P.F.(1996). Geometrical Observations of Turbulent Interfaces. *The mathemetics of deforming surfaces.* IMA, Oxford. 1996., pp 1-11. 1985a.

10. Gade M. and Redondo J.M.(1999). Marine pollution in European coastal waters monitored by the ERS-2 SAR: a comprehensive statistical analysis". IGARSS 99. Hamburg. v. III, 1637-1639. 308-312.

13. Dalziel S. and Redondo J.M. (2007). New visualization and self-similar analysis in experimental turbulence studies, *Models, Experiments and Computation in Turbulence,* R. Castilla, E. Oñate and J.M. Redondo (Eds.), CIMNE, Barcelona.

14. J.M. Redondo, A. Matulka, A. Carrillo and R. Castilla. (2008)Turbulent diffusion in strongly stratified and rotating flows. *Topics in Fluid Dynamics*, (Ed. Prihoda I and Kozel K.) 124-129. CAS, Prague.

15. Platonov A, A. Tarquis, E. Sekula and J. M. Redondo (2007). SAR observations of vertical structures and turbulence in the ocean. *Models, Experiments and Computation in Turbulence,* R. Castilla, E. Oñate and J.M. Redondo (Eds.), CIMNE, Barcelona..

16. Mahjoub O.B. Redondo J.M. and Babiano A. (2000) Structure functions in complex flows, *Journal of Flow Turbulence and Combustion* 59, 299-313.

17. Mahjoub O. B., Granata T. and Redondo J. M.(2001). Scaling laws in geophysical flows, *Phys. Chem. Earth (B),* 26, 281-285.